PAPER

Environmentally friendly fabrication of Ag nanoparticles decorated on g-C$_3$N$_4$ for enhancing the photodegradation of RhB†

Lan Anh Luu Thi,[a] Quoc Tung Trieu,[a] Thi Hue Trinh,[b] Tuyet Mai Nguyen Thi,[c] Cong Tu Nguyen, [ID] [a] Tran Thanh Tung [ID] [d] and Nguyen Xuan Sang [ID] *[ef]

This work presents an eco-friendly method for the preparation of a silver nanoparticle (AgNP) decorated g-C$_3$N$_4$ nanocomposite using purple leaf extract as a green reduction agent. The photocatalytic performance of the resulting nanocomposite was studied through the degradation of rhodamine B (RhB) dye pollution in an aqueous solution. X-ray diffraction analysis of powder samples revealed the coexistence of face-centered cubic AgNP crystalline and g-C$_3$N$_4$ structures, with a slight shift in the dominant diffraction peak (002) of g-C$_3$N$_4$, indicating successful incorporation of AgNPs. Optical analysis showed a reduction in the bandgap of the nanocomposite compared with that of the pure g-C$_3$N$_4$ sample. The photocatalytic ability of the nanocomposites was tested through the degradation of RhB dye, which was significantly enhanced by the presence of AgNPs, achieving a maximum degradation efficiency of approximately 95.3% after only 75 minutes of irradiation using the Ag@g-C$_3$N$_4$ nanocomposite with 7 wt% AgNPs as a photocatalyst. This enhancement is attributed to the efficient charge carrier separation and suppressed recombination rate at the photocatalyst interfaces.

1. Introduction

Organic dyes, especially synthetic organic dyestuffs, are widely used across various industries, including textile dyeing, printing, leather processing, papermaking, and cosmetics, to meet both individual and societal demands.[1] Most dyes possess complex structures and high molecular weights, are water soluble and are barely biodegradable, thus posing a serious threat to the environment.[2] Currently, environmental treatment in general and wastewater treatment in particular have become a hotspot not only in basic research but also in applied research, and increasing research focuses on removing pollutants from water using new technologies.[3–8] For the survival of humans and other living organisms, it is important to decompose dyes in an environmentally friendly and highly efficient way. Among the various approaches explored, photocatalysis has gained considerable attention. In this context, recently, graphitic carbon nitride (g-C$_3$N$_4$) has emerged as a potential photocatalyst that has been extensively studied[9–11] due to its unique properties, such as high thermal and chemical stabilities, abundant and low-cost building elements, environmental friendliness, and especially a suitable electronic structure with band edges straddling the water redox potentials, making it highly suitable for application in photocatalysis.[12–14] g-C$_3$N$_4$ is a polymer semiconductor that has been widely used in photocatalytic research because of its outstanding activity for various catalytic reactions, such as the decomposition of organic pollutants,[15] producing H$_2$ and O$_2$ by splitting water[16] and reducing CO into organic fuels.[17] However, the high recombination rate of photogenerated electron–hole pairs and limited active sites limit the applications of this material.[18]

Various methods, including increasing the surface area, reducing the electron–hole recombination rate and extending the visible light absorption region to longer wavelengths, are among the studies that have been carried out to improve the photocatalytic activity of g-C$_3$N$_4$. One of the effective solutions to separate the electron–hole pairs and prevent their recombination is to create composite materials using g-C$_3$N$_4$ and other metal nanoparticles. This hybridization significantly reduces electron–hole recombination as noble metal nanoparticles can serve as efficient electron acceptors due to their strong surface plasmon resonance effect.[19,20] To enhance the photocatalytic

[a]Faculty Engineering of Physics, Hanoi University of Science and Technology, No. 1, Dai Co Viet Street, Hai Ba Trung District, 100000 Hanoi, Vietnam

[b]Faculty of Electronics and Telecommunications, Electric Power University, No. 235 Hoang Quoc Viet Street, Hanoi, Vietnam

[c]School of Chemistry and Life Sciences, Hanoi University of Science and Technology, No. 1, Dai Co Viet Street, Hai Ba Trung District, 100000 Hanoi, Vietnam

[d]The University of Adelaide, School of Chemical Engineering, Adelaide, SA 5005, Australia

[e]Atomic Molecular and Optical Physics Research Group, Institute for Advanced Study in Technology, Ton Duc Thang University, Ho Chi Minh City, Vietnam. E-mail: nguyenxuansang@tdtu.edu.vn

[f]Faculty of Electrical and Electronics Engineering, Ton Duc Thang University, Ho Chi Minh City, Vietnam

† Electronic supplementary information (ESI) available. See DOI: https://doi.org/10.1039/d5na00552c

activity, other semiconductor oxides such as TiO_2 can also be modified with Ag to reduce contaminants in an aqueous phase.[21] The doping, hybridization, modification or compositing of Ag with g-C_3N_4 may change the conductivity of the composite material compared to that of pure g-C_3N_4 due to the reduction of the energy barrier for the transfer of electrons. Pham *et al.* reported the fabrication of Ag/g-C_3N_4 material *via* a photoreduction method. The 20% Ag/g-C_3N_4 sample provides the highest photocatalytic efficiency of NO decomposition and reaches 80% under visible light irradiation.[22] Dong Liang *et al.* prepared Ag/g-C_3N_4 for which the g-C_3N_4 was synthesized by urea pyrolysis at 550 °C with a heating rate of 15 °C min^{-1} for 3 h. The obtained results showed that the photocatalytic nitration of pharmaceutical intermediate halo-nitro-phenol, using various bromophenols and nitrites as raw materials, was significantly improved when using Ag/g-C_3N_4 composite as the photocatalyst compared with pure g-C_3N_4.[23] In another work, the Ag/g-C_3N_4 composite was synthesized *via* polymerization and the silver mirror reaction. In the sample surveys, the sample containing 5% Ag had the highest hydrogen production rate which was 39 times higher than that of bulk g-C_3N_4 with a value of 568.9 $\mu mol\ g^{-1}\ h^{-1}$.[24] Hai Zhu *et al.* used an ultrasound-assisted method to prepare Ag/g-C_3N_4 catalysts for photocatalytic water splitting. The results showed that the optimal synthesis conditions were 60 W ultrasonic power for 35 s (residence time). The sample showing the best photocatalytic activity for the water splitting reaction was the 7 wt% Ag/g-C_3N_4 sample, which had a reaction rate constant 2.76 times higher than that of pristine g-C_3N_4.[25]

In this study, Ag was selected to investigate its interaction with g-C_3N_4 and its influence on the structural, physical and chemical properties and photocatalytic ability of g-C_3N_4. The photocatalytic activity was examined through the degradation of RhB dye. In addition, the effects of reaction parameters on the photocatalytic performance and the photocatalytic enhancement mechanism were systematically evaluated.

2. Experimental

2.1 Chemical materials

Urea was purchased from Sigma and silver nitrate was purchased from Xilong Scientific Co., Ltd (China). Double distilled water (Aquatron A4000D) was used in all experiments. All chemicals were used as received without further purification.

2.2 Synthesis of Ag@g-C_3N_4 nanocomposites

The g-C_3N_4 was synthesized from urea using a thermal condensation method, as follows. 40 g of urea was placed in a crucible with a lid, then the sample was annealed at 500 °C for 2 h with a heating rate of 5 °C min^{-1}. The product achieved is g-C_3N_4 in light yellow bulk form. Purple leaves were extracted according to the procedure described in the ref. 26.
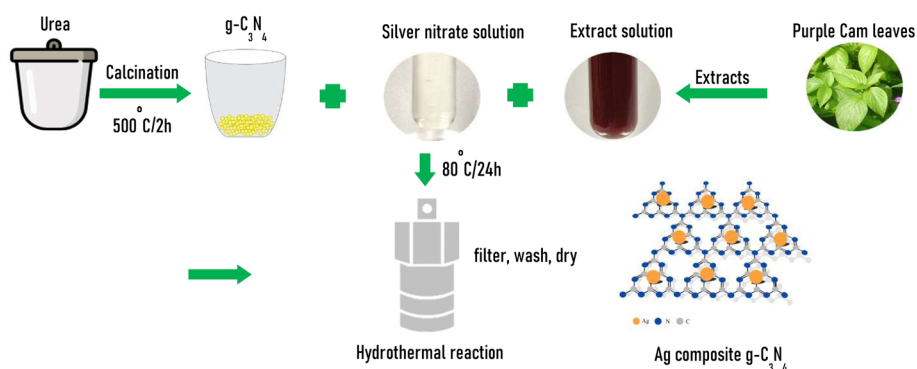
For the synthesis of Ag@g-C_3N_4 nanocomposites, predetermined amounts of $AgNO_3$ and g-C_3N_4 were dissolved into 50 ml of purple leaf extract under the effect of magnetic stirring for about 60 minutes to obtain 50 ml of precursor suspension solution. This solution was transferred to a 100 ml hydrothermal autoclave. The hydrothermal reaction was performed at 80 °C for 24 h. The suspension obtained after the reaction was washed several times with distilled water to remove the by-products, and the samples were dried at 80 °C for 24 h. The experimental scheme is illustrated in Scheme 1. The Ag@g-C_3N_4 nanocomposites were designated according to their Ag contents as summarized in Table 1. The obtained samples are denoted as g-C_3N_4, ACN03, ACN07, ACN10 and ACN20, respectively, corresponding to the Ag contents in the synthesized samples of 3, 7, 10, and 20 weight percentage.

2.3 Analysis

The structural characteristics of the nanocomposites were analyzed from the XRD data of the powder samples using an

Table 1 Sample name and the corresponding mass percentage of silver used in the nanocomposites

Sample name	Weight percent of Ag (wt%)	Weight of g-C_3N_4 (g)	Weight of Ag (g)
g-C_3N_4	0	0.300	0.000
ACN03	3	0.291	0.009
ACN07	7	0.279	0.021
ACN10	10	0.270	0.030
ACN20	20	0.240	0.060

Scheme 1 Schematic of the preparation process of Ag@g-C_3N_4 nanocomposites.

X'pert Pro (PANalytical) MPD system with CuKα radiation (λ = 1.54065 Å), a scanning speed of 0.03° per 2 s, and 2θ values from 10° to 80°. The vibrational characteristics of the functional groups were found from the FTIR spectra and measured on a FT/IR-4600 TypeA system (JASCO) with wavenumbers from 500 cm^{-1} to 4000 cm^{-1}. The surface morphology of the nanocomposites was observed through FESEM (Hitachi S4800) and TEM image analysis (JEM1010-7600F, JEOL). The reflectance spectra of the nanocomposites were also examined using a JASCO V-750 system with an ISV-922 60 mm integrating sphere.

2.4 Photocatalytic studies

The photocatalytic properties of the nanocomposite samples were evaluated by their ability to degrade RhB dye under visible light irradiation. The assessment was conducted with a photocatalytic reaction chamber with an LED lamp (Highbay 150 W, SH-HB2-150 W, $\lambda \geq$ 450 nm). The details are as follows: 20 mg of Ag@g-C$_3$N$_4$ nanocomposite was well-dispersed into 50 ml of 10 ppm RhB solution. Then, the mixture was stirred in the dark for about 30 min to establish the adsorption and desorption equilibrium between the dye molecules and the photocatalyst surface. Next, the solution was illuminated by LED light. At certain time intervals, about 3 ml of the solution was taken out and centrifuged to separate the catalyst. The absorbance of the solution was measured using a UV-vis absorption spectrophotometer (Carry 100 double beam UV/vis spectrophotometer, VARIAN). In order to elucidate the photocatalytic degradation mechanism and identify the active species involved, radical scavenger experiments were conducted. Specific trapping agents such as isopropanol (1 mM), benzoquinone (1 mM) and sodium oxalate (1 mM) were individually added to the solution.

3. Results and discussion

3.1 Characterizations of the Ag@g-C$_3$N$_4$ (ACN) nanocomposite samples

The XRD patterns of the Ag@g-C$_3$N$_4$ nanocomposite samples measured in the 2θ angle range of 10°–80° are shown in Fig. 1a. In the as-prepared g-C$_3$N$_4$ sample, three diffraction peaks are observed at approximately 13.00°, 24.93° and 27.65°, attributed to the (100), (101) and (002) diffraction planes, respectively. These peaks are associated with the hexagonal phase of graphitic carbon nitride corresponding to the standard JCPDS card no. 87-1526.[27,28] In the Ag@g-C$_3$N$_4$ nanocomposite samples, additional diffraction peaks appear as the silver content increases, particularly up to 20 wt%. These new peaks are attributed to the FCC crystalline structure of silver, with the characteristic reflections at 2θ values of 38.1°, 44.3°, 64.4°, and 77.5° corresponding to the (111), (200), (220), and (311) planes, respectively.[26]

Furthermore, the characteristic diffraction peak position (002) of the g-C$_3$N$_4$ nanocomposite samples was observed to gradually shift slightly toward lower 2θ values when the amount of Ag increased. This may indicate the influence of Ag nanoparticles on the crystal structure of g-C$_3$N$_4$, potentially due to lattice distortion or interfacial interactions.

The vibrations of the organic functional groups in ACN nanocomposite samples were studied using FTIR spectroscopy, as shown in Fig. 1b. The absorption peaks observed at wavenumbers 1640, 1564, 1413, 1326, and 1247 cm^{-1} are attributed to the typical stretching vibrations of CN heterojunctions.[26,29] The vibration modes at wavenumbers 810 and 3169 cm^{-1} are due to the stretching vibrations of the triazine units and –NH, respectively. The wavenumber range from 3600 cm^{-1} to 3000 cm^{-1} corresponds to the O–H stretching vibration and a small amount of absorbed H$_2$O.[30,31] Furthermore, it was found that the shape of the FTIR spectra in all ACN samples remained almost unchanged.

Fig. 2 presents the FESEM images of the ACN nanocomposite samples. The as-prepared g-C$_3$N$_4$ sample exhibits a morphology of overlapping layered sheets, resembling a graphite-like structure. When silver nanoparticles decorate the g-C$_3$N$_4$ surface, a noticeable change in surface morphology is observed. As the amount of AgNPs in the nanocomposite sample increased, a progressive accumulation of Ag NPs on the g-C$_3$N$_4$ surface was evident, forming clusters of particles (samples ACN03, ACN07, ACN10 and ACN20).

To determine the silver content in the sample and compare it with theoretical calculations, the atomic compositions of the g-
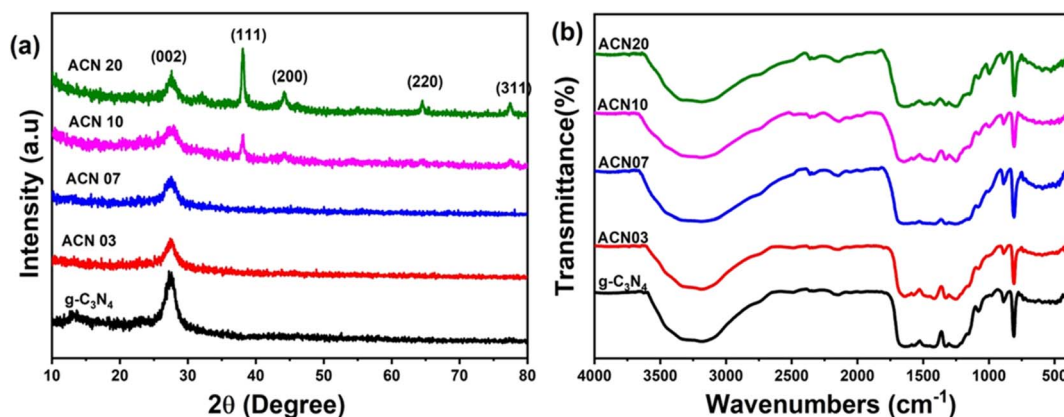

Fig. 1 (a) XRD patterns and (b) FT-IR spectra of ACN nanocomposite samples.
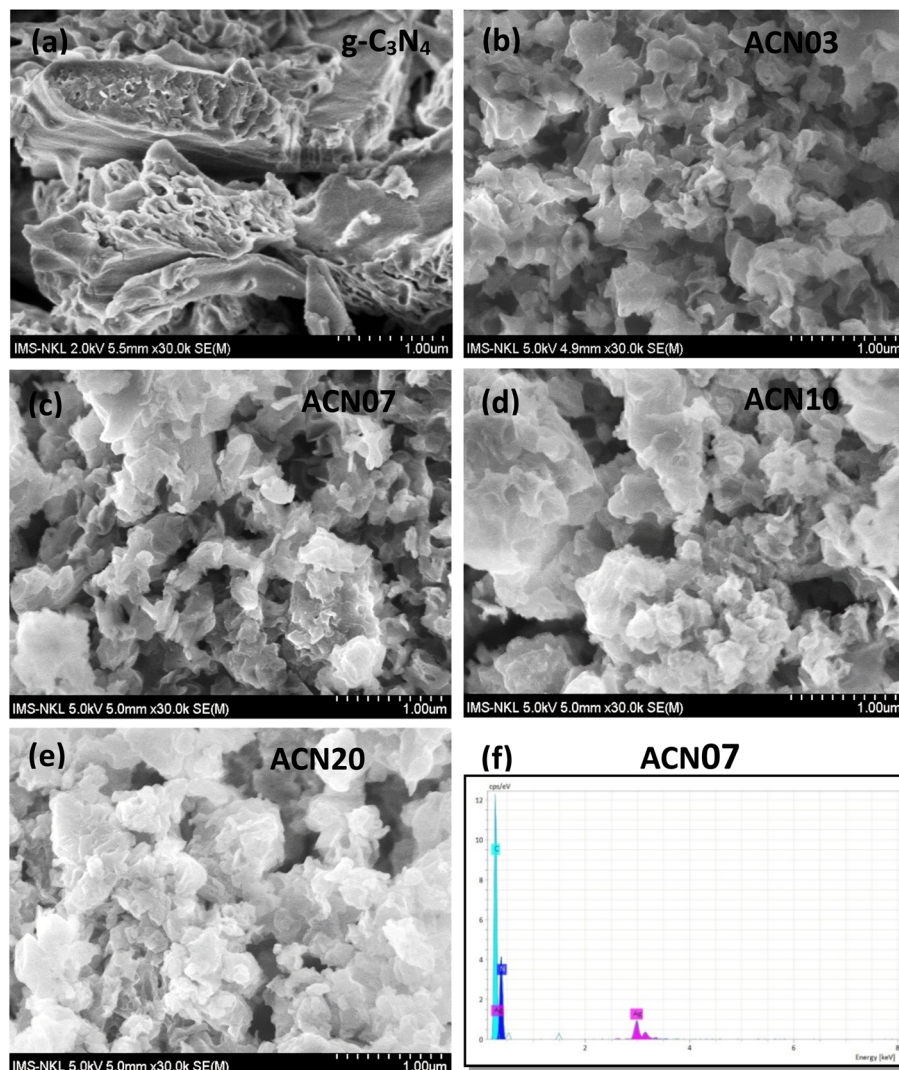
Fig. 2 FESEM images of the ACN nanocomposite samples: (a) g-C$_3$N$_4$, (b) ACN03, (c) ACN07, (d) ACN10, and (e) ACN20. (f) EDX spectrum of the ACN07 sample.

C$_3$N$_4$ and ACN07 samples were analyzed by energy dispersive X-ray spectroscopy (EDX). Fig. 2f shows the EDX spectrum results of the ACN07 sample. In the EDX spectrum, the characteristic peaks of the elements C, N and Ag appear, proving that in sample ACN07, there are elements C, N and Ag. Hence, the ACN nanocomposites possess high purity.

To further analyze the surface morphology of the composites, transmission electron microscopy (TEM) images of the CN and ACN07 samples were obtained and are shown in Fig. 3. The CN sample exhibits an uneven, layered structure with an irregular morphology. In contrast, the ACN07 sample shows the presence of small, dispersed particles which are attributed to the incorporation of Ag NPs into the g-C$_3$N$_4$ matrix.

Fig. 4a shows the reflectance spectra of the ACN nanocomposite samples. It is observed that the reflectance of the ACN nanocomposite samples remarkably increases when incorporating Ag nanoparticles. Moreover, the reflectance edge also shifts to a longer wavelength when the content of Ag increases, which implies more absorbance of visible light. The

reason for this redshift is believed to be due to the plasmonic properties of silver nanoparticles in nanocomposite samples, which effectively absorb most of the light in the visible and infrared regions.

To further study the optical properties of the nanocomposite samples and evaluate their efficiency in visible-light-induced applications such as photocatalysis under solar irradiation, the optical bandgaps of the nanocomposite samples were extracted from the derivative method based on the Kubelka–Munk equation[32,33] and expressed as

$$\frac{d[\ln(F(R)h\nu)]}{d(h\nu)} = \frac{n}{h\nu - E_g} \qquad (1)$$

where $F(R) = \frac{(1-R)^2}{2R}$ and $n = \frac{1}{2}$ or 2 for direct or indirect allowed recombination, respectively.[34]

The first derivative induced optical bandgaps of ACN nanocomposite are shown in Fig. 4b, and Fig. 4c shows that the optical band gap energy decreases with increasing silver content. This result might originate from the increase of
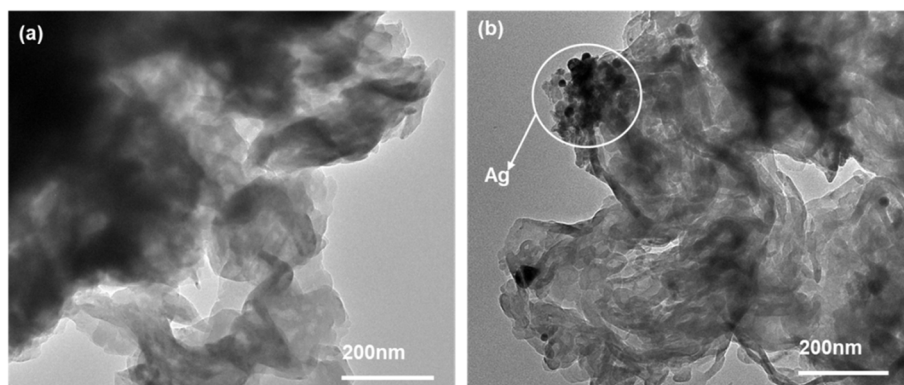
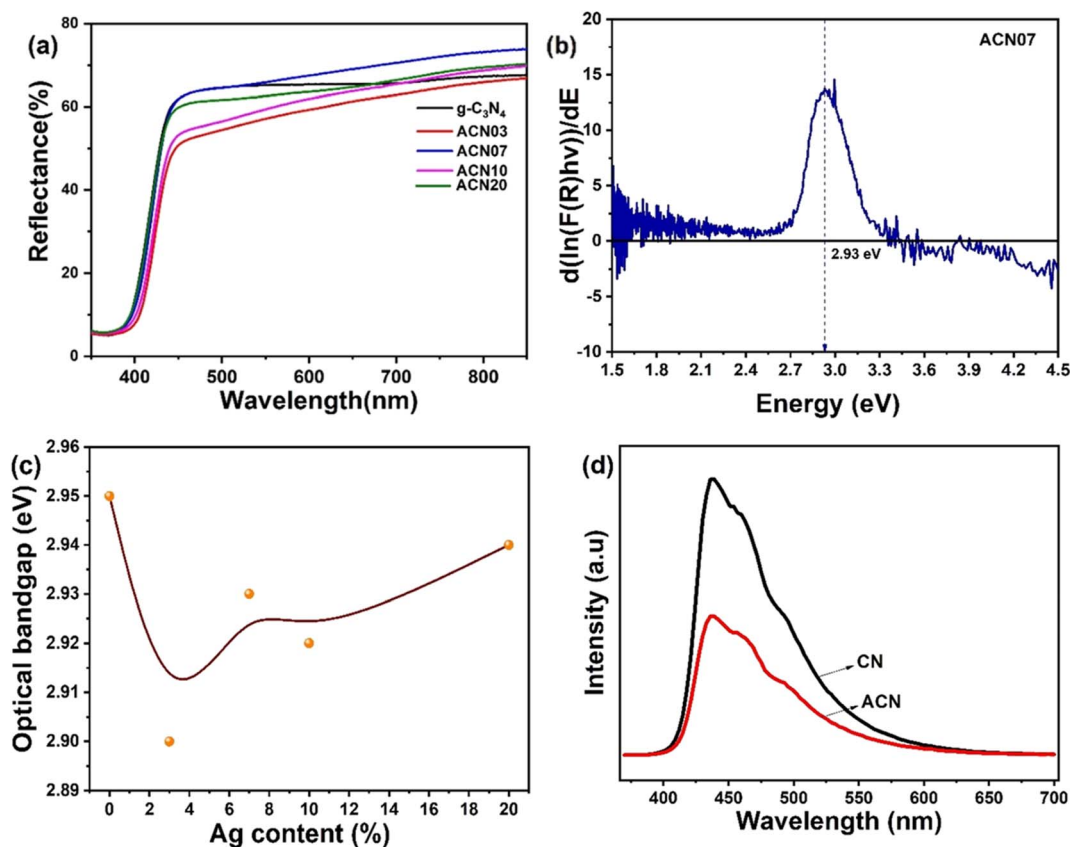Fig. 3   TEM images of (a) g-C$_3$N$_4$ and (b) ACN07.

Fig. 4   (a) Reflectance spectra. (b) Optical bandgaps of the ACN07 nanocomposite samples obtained by the first-derivative method. (c) Graph of optical bandgap *vs.* AgNPs content. (d) PL spectra of the ACN nanocomposite samples.

absorbance due to the plasmonic resonance properties of Ag in the nanocomposites.

The PL fluorescence spectra of g-C$_3$N$_4$ and ACN07 samples, shown in Fig. 4d, indicated that the maximum emission of g-C$_3$N$_4$ (CN) is ~435 nm and it has a higher intensity than the ACN07 sample, consistent with the results observed in the UV vis absorption spectra. This proves that the regeneration rate of photogenerated carriers in g-C$_3$N$_4$ is faster. In contrast, in the ACN07 sample, the recombination rate is slower or the lifetimes of electrons and holes are longer. This means that the

photocatalytic ability is enhanced, because the longer the electrons and holes exist, the more carriers participate in the toxic compound decomposition reactions, leading to higher treatment efficiency.

3.2   Photocatalytic activity of the Ag@g-C$_3$N$_4$ (ACN) nanocomposite samples in decomposing rhodamine B dye

The decrease in RhB concentration over the photocatalytic reaction time is shown in Fig. 5a. The dominant peak located at ~550 nm is assigned to the absorption peak of RhB.[35] As the
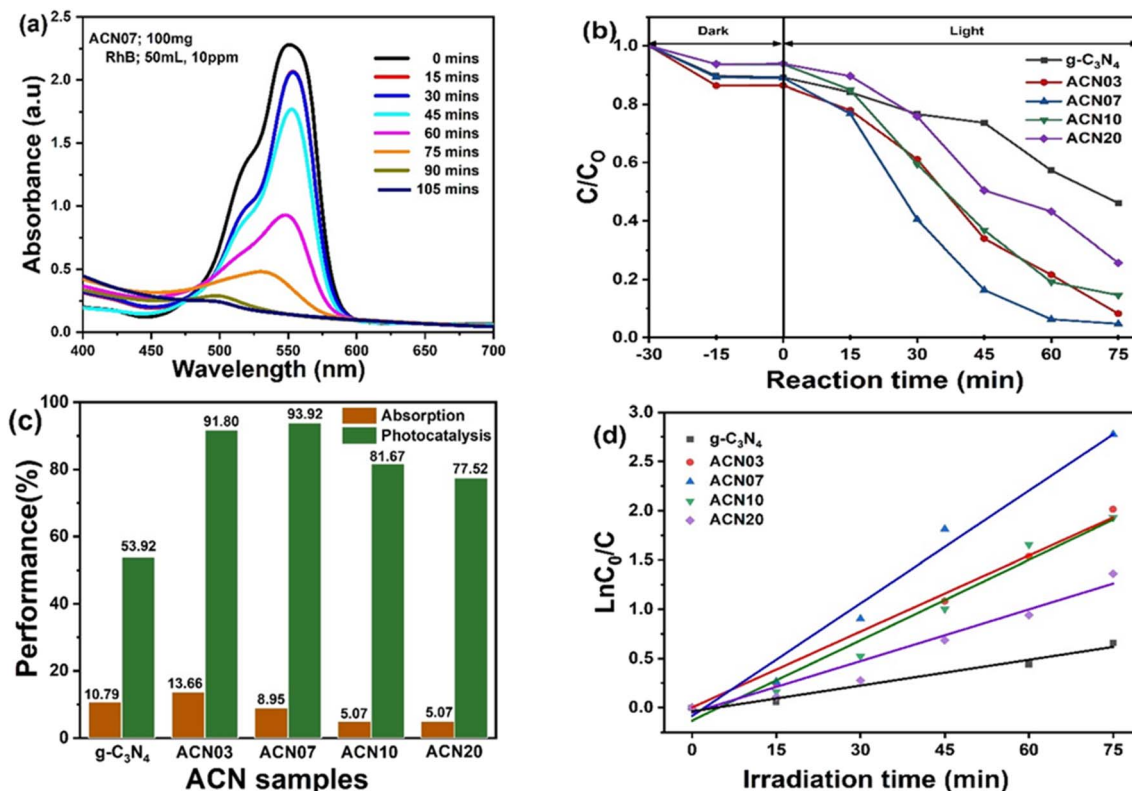
Fig. 5 (a) Sequence of RhB photodegradation on the ACN07 nanocomposite sample under visible-light irradiation. (b) Photodegradation of RhB at various reaction times under dark and visible light conditions. (c) Photodegradation performances for RhB on the ACN nanocomposite samples. (d) First-order kinetic curves of RhB decomposition on the ACN nanocomposite samples under visible-light irradiation.

reaction time progressed, the intensity of the RhB adsorption peak gradually decreased, indicating that the concentration of RhB in the solution gradually decreased. In other words, RhB was decomposed by photocatalytic reaction using ACN nanocomposite as the catalyst. Furthermore, the dominant peak was slightly blue-shifted by the time of irradiation corresponding to the color of the solution changing from pink-red to greenish-yellow. Hence, RhB was decomposed into intermediate substances.[36–38]

The graphs of RhB concentration dependence on reaction time are shown in Fig. 5b. Over 30 minutes, during adsorption–desorption equilibrium in the dark, RhB concentration decreased by about 5–15%. After 75 minutes of illumination, the RhB was almost completely decomposed. The ACN07 sample gives the fastest decomposition of RhB solution, with an efficiency of 93.9%, followed by samples ACN00 and ACN03, which are slightly lower at 92.2% and 91.7%. The ACN10 and ACN20 samples showed relatively low efficiencies, with 81.67% and 77.52% (Fig. 5c), respectively. Thus, the photocatalytic efficiency of the Ag@g-C$_3$N$_4$ nanocomposite sample depends on the Ag ratio.

The photocatalytic reaction rate is expressed through the Langmuir–Hinshelwood kinetic equation

$$r = \frac{\mathrm{d}C}{\mathrm{d}t} = \frac{kKC}{1 + KC} \quad (2)$$

where r is the reaction rate, C is the reactant concentration, t is the illumination time, k is a constant and K is the absorbance coefficient of the reactant. When the concentration of the substance is relatively small, the equation can be simplified to

$$-\ln\frac{C}{C_0} = kKt = k_{app}t \quad (3)$$

where k_{app} is the rate coefficient and is obtained from the slope of the linear function graph of the equation.

Fig. 5d shows the interpolated linear function according to the experimental data of each ACN nanocomposite sample and the R^2 coefficient. Table 2 gives the k_{app} rate constants and R^2 constants of the ACNx nanocomposite samples. The R^2 coefficients of all nanocomposite samples are greater than 0.97, so the Langmuir–Hinshelwood model relatively appropriately reflects the photocatalytic process for RhB of the ACN nanocomposite samples. The ACN07 sample has the best photocatalytic ability ($k = 0.039$ min^{-1}). It is possible that silver nanoparticles in nanocomposites act not only as an electron pool but also to capture the photoinduced electrons.

In the catalytic system, TON and TOF are two important parameters used to evaluate the lifetime and performance of a catalyst.[39] Therefore, TOF per unit amount of Ag NPs (Table 2) was used to evaluate the effect of Ag doping on the material properties. The ACN07 sample has the highest TOF of 30.76 min^{-1}. When the Ag doping amount increases, the TOF

Table 2 The activity, k_{app}, TON and TOF of ACNx nanocomposite samples

Sample	The content of Ag (wt%)	Activity (%)	k_{app} (min^{-1})	R^2	TON$_{Ag}$	TOF$_{Ag} \times 10^{-4}$ (min^{-1})
g-C$_3$N$_4$	0	53.92	0.009	0.986	—	—
ACN03	3	91.80	0.033	0.977	0.231	30.76
ACN07	7	93.92	0.039	0.970	0.101	13.49
ACN10	10	81.67	0.027	0.976	0.062	8.21
ACN20	20	77.52	0.019	0.980	0.029	3.90

decreases. This phenomenon occurs because when Ag increases, the amount of metal on the surface increases but its dispersion on the surface decreases. However, the opposite TON and TOF values also indicate that ACN has higher photocatalytic activity than pure g-C$_3$N$_4$. Therefore, there was a beneficial interaction between Ag and the g-C$_3$N$_4$ matrix. For details of the TON and TOF calculations, please see the ESI.†

The catalyst dosage also affects the dye decomposition efficiency. If the catalyst dosage is low, it is not enough to create active centers for the dye adsorption process on the catalyst surface, so the dye decomposition efficiency will decrease. If the catalyst dosage is too high, it will block the incident light and reduce light absorption, leading to a decrease in the ability to trap light and preventing the generation of photogenerated electrons and holes, so the dye decomposition efficiency will also decrease. Therefore, an optimal balance between RhB adsorption capacity and photon collection capacity will be achieved with the optimal catalyst dosage, and the efficiency will be optimized.

Fig. 6a presents the degradation of RhB using the ACN07 nanocomposite at different dosages (50–100 mg). The catalytic reaction rate was significantly enhanced with the dosage of catalyst. To evaluate the effect of dosage on the catalytic performance, the ratio of reaction rate to dosage was calculated. The performance ranking was as follows: 70 mg > 60 mg > 50 mg > 80 mg > 100 mg. Thus, the best sample dosage was 70 mg. Similarly, the RhB degradation reaction rate was affected by the concentration of RhB used (Fig. 6b). At low RhB concentration (5 ppm), the degradation rate of RhB increased significantly

compared to that at high concentration (30 ppm), because when the RhB concentration is too high, the adsorption of RhB onto the catalyst decreases. The optimal RhB concentration in this study was 10 ppm.

The photocatalytic performance of RhB decolourization largely depends on the generation of strong chemically active radicals during the reaction process. The primary active species typically considered include hydroxyl radicals ($^{\bullet}$OH), superoxide radicals ($^{\bullet}$O$_2^{-}$), and photogenerated holes (h^{+}). In this work, to study the effects of chemically active radicals, three agents were used: benzoquinone (BQ), isopropanol (IPA), and sodium oxalate (NO) for the radicals superoxide (*O$_2^{-}$), hydroxyl (*OH^{-}) and hole (h^{+}), respectively. In each experiment, 1 ml of the agent with a 1 mM concentration of the respective scavenger was added into a beaker containing 50 ml of 10 ppm RhB solution containing 0.07 g ACN07. The corresponding decolourization efficiencies in the presence of the agents are shown in Fig. 7a.

The role of reactive species in the photocatalytic degradation of RhB was further investigated through radical scavenging experiments. The addition of isopropanol has little effect on the reaction rate. Thus, it can be confirmed that the hydroxyl radical (*OH^{-}) is not essential in the decomposition process of RhB dye. Interestingly, in the presence of the NO scavenger, the photocatalytic activity of the Ag@g-C$_3$N$_4$ nanocomposite sample increases, so h^{+} is not the active substance in this photodegradation process. In the presence of BQ, the reaction rate decreased the most. At the same time, it was observed that the peak shift phenomenon occurred relatively little, but the spectrum gradually increased with illumination time. The spectral
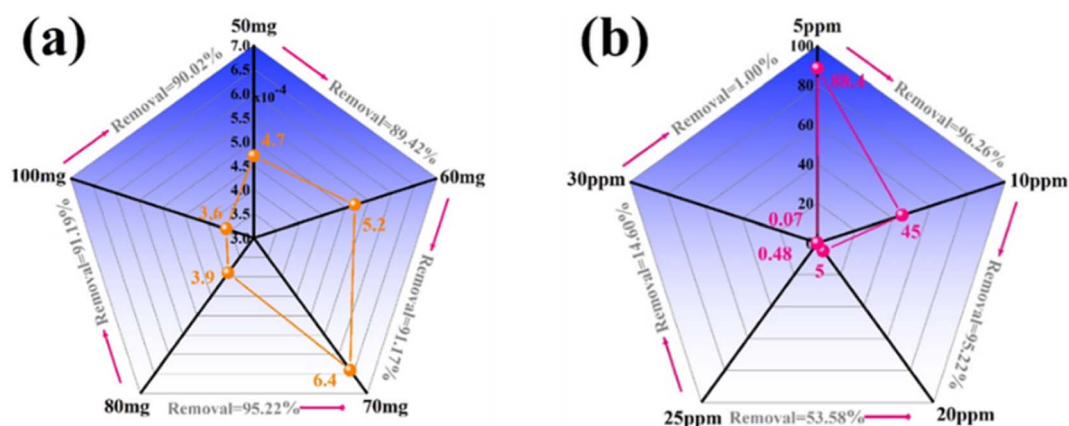

Fig. 6 Effects of (a) the dosage of ACN07 and (b) concentration of RhB solution on photocatalytic activity.
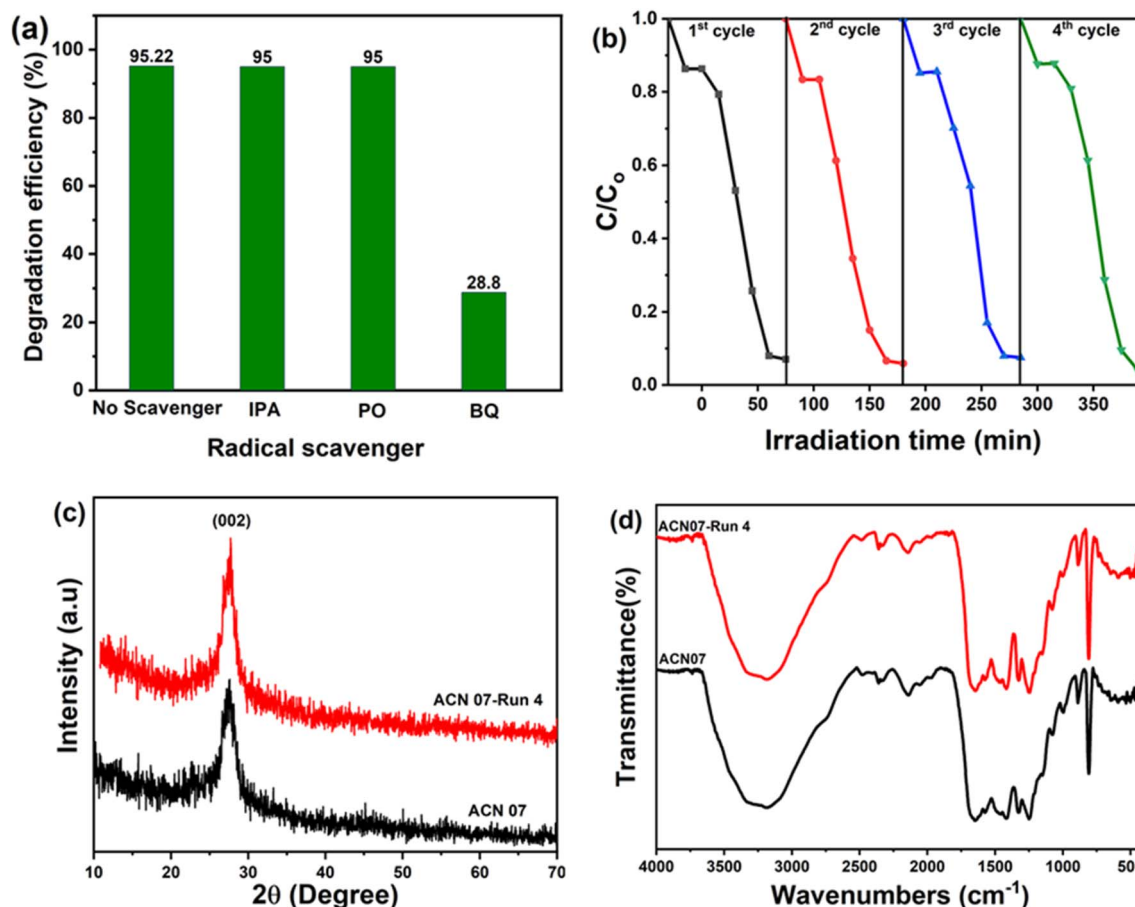
Fig. 7   (a) Effect of scavengers. (b) Cycling runs, (c) XRD patterns and (d) FT-IR spectra of the ACN07 sample initially and after the fourth cycle.

enhancement becomes stronger when moving towards short wavelengths. The photodegradation of the RhB dye was significantly inhibited in the presence of BQ, demonstrating that O_2^- plays a major role in this process.

These results demonstrate that h^+ and especially O_2^- are the main reactants in the photocatalytic RhB decomposition. The reusability of the Ag@g-C_3N_4 photocatalyst was evaluated by four consecutive photocatalytic runs, as seen in Fig. 7b. For each recycling, the photocatalytic material was filtered using a vacuum system to collect the residue. The resulting residue was dried in a dryer at 80 °C for 24 h. Then, the material was ground and photocatalyzed under similar conditions (material weight 0.07 g, RhB dye volume 50 ml at 10 ppm concentration).

RhB photodegradation efficiency was almost complete in each cycle. Therefore, there was no significant loss of catalytic activity even after 4 cycles. Therefore, the Ag@g-C_3N_4 nanocomposite is reusable.

Fig. 7c and d show the XRD and FTIR results of the ACN07 sample initially and after the cycling. It is easy to see that the diffraction peaks of the ACN07 sample hardly change after 4 cycles (Fig. 7c). This means that the ACN07 sample has good repeatability and stability. The FTIR measurement results of this sample are consistent with the XRD measurement results.

The photocatalytic enhancement mechanism of RhB degradation by ACN nanocomposite can be described as shown in Fig. 8. The E_{VB} and E_{CB} values of the Ag@g-C_3N_4 nanocomposites can be calculated by the equations[40]

$$E_{VB} = X + 0.5E_g - E_e,$$
$$E_{CB} = E_{VB} - E_g, \qquad (4)$$

where E_{VB} is the valence band potential, E_{CB} is the conduction band potential, X is the absolute electronegativity of the semiconductor and E_e is the energy of free electrons on the hydrogen scale ($E_e = 4.5$ eV). The X value for g-C_3N_4 is 4.73 eV. E_g is the optical band gap of Ag@g-C_3N_4. In this case, $E_g = 2.93$ eV (ACN07).

The values of E_{CB} and E_{VB} for g-C_3N_4 are estimated to be −1.24 eV and 1.70 eV, respectively.

The reaction process is described in eqn (5)–(8) and is detailed as follows. Under the irradiation of visible light, only g-C_3N_4 absorbs visible light and is excited. Then, the electrons in the VB can be transferred to the CB of g-C_3N_4 to generate photogenerated electron pairs. Due to the SPR effect of silver in the form of nanoparticles, the generation rate of e–h pairs of g-C_3N_4 increases.[41,42] Finally, the $^\cdot O_2^-$ species photodegraded RhB into H_2O and CO_2 as follows.

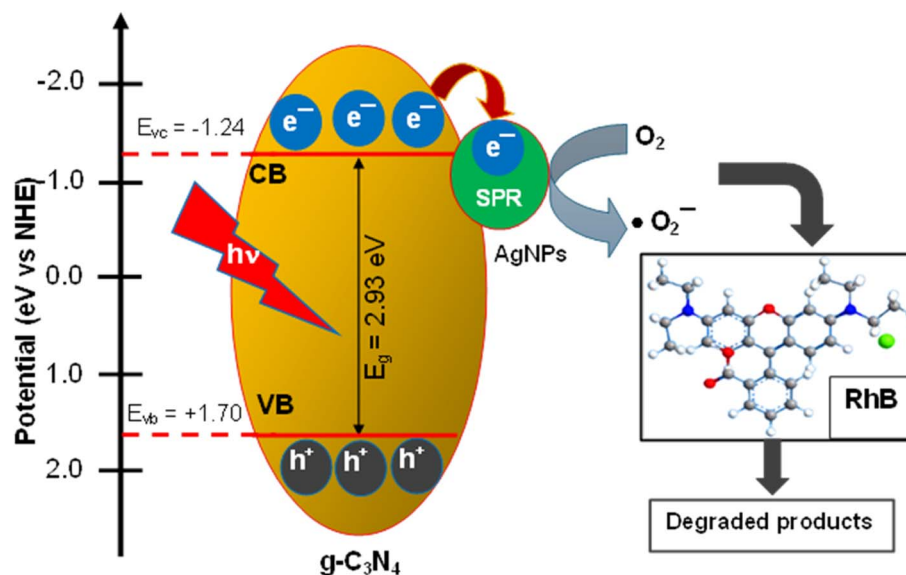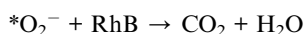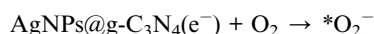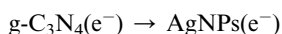$$\text{g-}C_3N_4 + h\nu \rightarrow \text{g-}C_3N_4(e^- + h^+) \qquad (5)$$
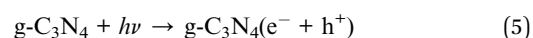
Fig. 8 Proposed mechanism for the improved photocatalytic behaviour toward RhB over the ACN composite under LED illumination.

Table 3 Photocatalytic degradation of the RhB dye under visible light

Photocatalyst	Light source	Dosage (mg)	Dye concentration (ppm)	Volume of dye (ml)	Reaction time (min)	Removal efficiency (%)	Ref.
Ag-(P/CNNS)	Xe lamp 300 W	25	10	50	240	98	43
a-AgSiO/CNNS-500	Xe lamp 500 W	50	10	50	150	95	44
Ag@g-C$_3$N$_4$ NSs	Xe lamp 400 W	2	10	20	250	89	45
0.02Ag/g-C$_3$N$_4$	100 W	20	5	100	25	97	46
AgI/g-C$_3$N$_4$	Osram, 125 W	50	5	50	120	80	47
ACN07	LED lamp, 150 W	70	10	50	75	95	This work

$$g\text{-}C_3N_4(e^-) \rightarrow AgNPs(e^-) \qquad (6)$$

$$AgNPs@g\text{-}C_3N_4(e^-) + O_2 \rightarrow {}^*O_2^- \qquad (7)$$

$${}^*O_2^- + RhB \rightarrow CO_2 + H_2O \qquad (8)$$

Table 3 summarizes the RhB degradation performance of the ACN07 sample compared with some published results. ACN07 has a very good RhB degradation efficiency of up to 95% in 75 min. Moreover, the reaction can be carried out with an LED lamp (150 W, $\lambda \geq 450$ nm). The sample has high stability after 4 cycles. The results indicate the applicability of ACN samples in wastewater treatment.

4. Conclusion

In summary, AgNPs@g-C$_3$N$_4$ nanocomposites were successfully synthesized through a thermal hydrolysis method at low temperatures using purple leaf extract as a reducing agent and solvent. The resulting nanocomposite materials showed significantly enhanced photocatalytic activity compared to pure g-C$_3$N$_4$, primarily due to the surface plasma resonance (SPR) effect of the Ag NPs, and a reduced recombination rate of the photogenerated e$^-$–h$^+$ pairs. Among the series of photocatalysts, the ACN07 sample demonstrated the highest photocatalytic efficiency, achieving a RhB degradation rate of 95.3% under visible light irradiation. The optimal parameters for the photocatalytic process were identified as 0.7 g of ACN07 in 50 ml of 10 ppm RhB solution irradiated for 75 minutes of illumination using an LED lamp, and the photocatalyst remained stable after 4 cycles. The experiment also showed that the main agent enhancing the photocatalytic activity of the ACN nanocomposite is the super oxygen free radical.

Data availability

The data supporting this article have been included as part of the ESI.†

Author contributions

Nguyen Xuan Sang: writing – original draft, writing – review & editing, visualization, validation, supervision, and conceptualization. Quoc Tung Trieu: data curation, software, methodology, investigation, and formal analysis. Thi Hue Trinh: data curation, methodology, investigation, and formal analysis. Thi Tuyet

Mai Nguyen: validation, resources, investigation, formal analysis, and conceptualization. Cong Tu Nguyen: writing – original draft, writing – review & editing, visualization, validation, supervision, and conceptualization. Tran Thanh Tung: writing – review & editing, visualization, validation, and conceptualization. Thi Lan Anh Luu: supervision, methodology, writing – original draft, writing – review & editing, conceptualization, and funding acquisition.

Conflicts of interest

The authors declare that they have no known competing financial interests or personal relationships that could have influenced the work reported in this paper.

Acknowledgements

References

1 X. Lai, et al., Rapid microwave-assisted bio-synthesized silver/Dandelion catalyst with superior catalytic performance for dyes degradation, J. Hazard. Mater., 2019, **371**, 506–512, DOI: 10.1016/j.jhazmat.2019.03.039.

2 R. Banu, D. Ramakrishna, G. B. Reddy, G. Veerabhadram and K. G. Mangatayaru, Facile one-pot microwave-assisted green synthesis of silver nanoparticles using Bael gum: Potential application as catalyst in the reduction of organic dyes, Mater. Today: Proc., 2020, **43**, 2265–2273, DOI: 10.1016/j.matpr.2020.12.861.

3 N. Yahya, F. Aziz, N. A. Jamaludin, J. Jaafar, N. Yusof and N. A. Ludin, A review of integrated photocatalyst adsorbents for wastewater treatment, J. Environ. Chem. Eng., 2018, **6**(6), 7411–7425, DOI: 10.1016/j.jece.2018.06.051.

4 A. Siddique, M. Shaheen, A. Abbas, Y. Zaman, M. Ishaque, A. Shami, M. Aslam, K. Alsyaad and A. Ali, Highly efficient greenly synthesized cadmium oxide nanoparticles for methyl orange degradation, antibacterial and antioxidant applications, J. Mol. Struct., 2025, **1331**, 141566, DOI: 10.1016/j.molstruc.2025.141566.

5 A. B. Siddique, et al., Optimization of photodegradation of crystal violet dye and biomedical applications of greenly synthesized NiO nanoparticles, Mater. Adv., 2024, 1330–1344, DOI: 10.1039/d4ma01078g.

6 D. Patel, K. M. Tripathi and R. K. Sonwani, Waste-Derived Carbon Nano-Onions for the Removal of Organic Dye from Wastewater and Phytotoxicity Studies, ACS Omega, 2024, **9**(28), 30834–30845, DOI: 10.1021/acsomega.4c03570.

7 H. Asati, R. Mondal and K. M. Tripathi, Economically viable N-doped graphene aerogel for the photodegradation of structurally different dyes and a plant-model-based environmental assessment, Environ. Sci.: Nano, 2024, **11**, 969–982, DOI: 10.1039/D3EN00752A.

8 N. Dhiman, V. K. Tripathi, J. Dwivedi, R. K. Gupta and K. M. Tripathi, Photoactive Graphene Aerogel from Biomass for the Visible-Light-Induced Degradation of Pharmaceutical Residues, ACS Sustainable Resour. Manage., 2024, **1**(6), 1068–1075, DOI: 10.1021/acssusresmgt.3c00088.

9 M. Raaja Rajeshwari, S. Kokilavani and S. Sudheer Khan, Recent developments in architecturing the g-C$_3$N$_4$ based nanostructured photocatalysts: Synthesis, modifications and applications in water treatment, Chemosphere, 2022, **291**(P1), 132735, DOI: 10.1016/j.chemosphere.2021.132735.

10 N. Q. Thang, A. Sabbah, L. C. Chen, K. H. Chen, C. M. Thi and P. Van Viet, High-efficient photocatalytic degradation of commercial drugs for pharmaceutical wastewater treatment prospects: A case study of Ag/g-C$_3$N$_4$/ZnO nanocomposite materials, Chemosphere, 2021, **282**, 130971, DOI: 10.1016/j.chemosphere.2021.130971.

11 K. R. Reddy, C. V. Reddy, M. N. Nadagouda, N. P. Shetti, S. Jaesool and T. M. Aminabhavi, Polymeric graphitic carbon nitride (g-C$_3$N$_4$)-based semiconducting nanostructured materials: Synthesis methods, properties and photocatalytic applications, J. Environ. Manage., 2019, **238**, 25–40, DOI: 10.1016/j.jenvman.2019.02.075.

12 M. Tan, et al., Engineering of g-C$_3$N$_4$-based photocatalysts to enhance hydrogen evolution, Adv. Colloid Interface Sci., 2021, **295**, 102488, DOI: 10.1016/j.cis.2021.102488.

13 R. Ahmad, et al., Review—Recent Advances in Nanostructured Graphitic Carbon Nitride as a Sensing Material for Heavy Metal Ions, J. Electrochem. Soc., 2020, **167**(3), 037519, DOI: 10.1149/2.0192003jes.

14 X. Zhang, X. Zhang, P. Yang and S. Ping Jiang, Transition metals decorated g-C$_3$N$_4$/N-doped carbon nanotube catalysts for water splitting: A review, J. Electroanal. Chem., 2021, **895**, 115510, DOI: 10.1016/j.jelechem.2021.115510.

15 Y. Chen and X. Bai, A review on quantum dots modified g-C$_3$N$_4$-based photocatalysts with improved photocatalytic activity, Catalysts, 2020, **10**(1), 142, DOI: 10.3390/catal10010142.

16 R. Mehmood, et al., 2D–2D heterostructure g-C$_3$N$_4$-based materials for photocatalytic H$_2$ evolution: Progress and perspectives, Front. Chem., 2022, **10**, 1–13, DOI: 10.3389/fchem.2022.1063288.

17 Y. Li, M. Zhang, L. Zhou, S. Yang, Z. Wu and Y. Ma, Recent advances in surface-modified g-C$_3$N$_4$-based photocatalysts for H$_2$ production and CO$_2$ reduction, Wuli Huaxue Xuebao, 2021, **37**(6), 1–15, DOI: 10.3866/PKU.WHXB202009030.

18 A. Balakrishnan and M. Chinthala, Comprehensive review on advanced reusability of g-C$_3$N$_4$ based photocatalysts for the removal of organic pollutants, Chemosphere, 2022, **297**, 134190, DOI: 10.1016/j.chemosphere.2022.134190.

19 A. Sudhaik, P. Raizada, P. Shandilya, D. Y. Jeong, J. H. Lim and P. Singh, Review on fabrication of graphitic carbon nitride based efficient nanocomposites for photodegradation of aqueous phase organic pollutants, J. Ind. Eng. Chem., 2018, **67**, 28–51, DOI: 10.1016/j.jiec.2018.07.007.

20 W. Yan, L. Yan and C. Jing, Impact of doped metals on urea-derived g-C$_3$N$_4$ for photocatalytic degradation of antibiotics: Structure, photoactivity and degradation mechanisms, Appl.

Catal., *B*, 2019, **244**, 475–485, DOI: **10.1016/j.apcatb.2018.11.069**.

21 P. T. Thuy, *et al.*, Local Surface Plasmonic Resonance, Surface-Enhanced Raman Scattering, Photoluminescence, and Photocatalytic Activity of Hydrothermal Titanate Nanotubes Coated with Ag Nanoparticles, *J. Nanomater.*, 2021, **2021**, 1–9, DOI: **10.1155/2021/3806691**.

22 M. T. Pham, T. M. T. Nguyen, D. P. Bui, Y. F. Wang, H. H. Tran and S. J. You, Enhancing quantum efficiency at Ag/g-C_3N_4 interfaces for rapid removal of nitric oxide under visible light, *Sustainable Chem. Pharm.*, 2022, **25**, 1–9, DOI: **10.1016/j.scp.2021.100596**.

23 D. Liang, *et al.*, Photocatalytic ipso-nitration of bromophenol intermediates on Ag/g-C_3N_4, *Sustainable Chem. Pharm.*, 2023, **33**, 101077, DOI: **10.1016/j.scp.2023.101077**.

24 T. Ren, *et al.*, Depositing Ag nanoparticles on g-C_3N_4 by facile silver mirror reaction for enhanced photocatalytic hydrogen production, *Inorg. Chem. Commun.*, 2021, **123**, 108367, DOI: **10.1016/j.inoche.2020.108367**.

25 H. Zhu, K. J. Wu and C. H. He, Ultrasound-assisted synthesis of visible-light-driven Ag/g-C_3N_4 catalysts in a continuous flow reactor, *Chem. Eng. J.*, 2022, **429**, 132412, DOI: **10.1016/j.cej.2021.132412**.

26 T. L. A. Luu, C. C. Nguyen, V. T. Pham, T. T. Tran, T. N. Nguyen, V. T. Phi and C. T. Nguyen, Green synthesis of Ag@AgCl nanoparticles using purple Cam leaf: characterization and catalytic activity, *Bull. Mater. Sci.*, 2023, **46**(3), DOI: **10.1007/s12034-023-02968-6**.

27 S. Hmamouchi, A. El Yacoubi, M. El Hezzat, B. Sallek and B. C. El Idrissi, Optimization of photocatalytic parameters for MB degradation by g-C_3N_4 nanoparticles using Response Surface Methodology (RSM), *Diamond Relat. Mater.*, 2023, **136**, 109986, DOI: **10.1016/j.diamond.2023.109986**.

28 M. Talukdar, R. Kuthethur, S. Banik, N. Mazumder, S. Chakrabarty and P. Deb, Biocompatible graphitic carbon nitride based fluorescent probe for imaging of breast cancer cell, *Mater. Lett.*, 2023, **333**, 133674, DOI: **10.1016/j.matlet.2022.133674**.

29 L. M. Cuong, *et al.*, Kinetics and Adsorption Model of Methylene Blue on g-C_3N_4@WO_3.H_2O Nanoplate Composite, *Int. J. Nanosci.*, 2021, **20**(5), 1–10, DOI: **10.1142/S0219581X21500459**.

30 L. Zhou, W. Zhang, L. Chen and H. Deng, Z-scheme mechanism of photogenerated carriers for hybrid photocatalyst Ag_3PO_4/g-C_3N_4 in degradation of sulfamethoxazole, *J. Colloid Interface Sci.*, 2017, **487**, 410–417, DOI: **10.1016/j.jcis.2016.10.068**.

31 D. Zhou and C. Qiu, Study on the effect of Co doping concentration on optical properties of g-C_3N_4, *Chem. Phys. Lett.*, 2019, **728**, 70–73, DOI: **10.1016/j.cplett.2019.04.060**.

32 T. D. Phan, C. M. Vo, T. M. T. Tran, T. L. A. Luu and X. S. Nguyen, Structural and bandgap properties of titanium dioxide nanotube/graphene oxide composites prepared by a facile hydrothermal method, *Mater. Res.*

Express, 2019, **6**(10), 105054, DOI: **10.1088/2053-1591/ab3a0b**.

33 N. X. Sang, *et al.*, Engineering of ZnO/Graphene Nanocomposite for Enhancing Visible Photocatalytic Ability, *Phys. Status Solidi A*, 2022, **219**(24), 1–10, DOI: **10.1002/pssa.202200172**.

34 C. T. Nguyen, *et al.*, Constraint effect caused by graphene on in situ grown Gr@WO_3-nanobrick hybrid material, *Ceram. Int.*, 2020, **46**(7), 8711–8718, DOI: **10.1016/j.ceramint.2019.12.108**.

35 H. Yamashita, A. Tanaka, M. Nishimura, K. Koyano, T. Tatsumi and M. Anpo, *Photochemical Properties of Rhodamine-B Dye Molecules Included within Mesoporous Molecular Sieves*, Elsevier Masson SAS, 1998, vol. 117, DOI: **10.1016/s0167-2991(98)81037-9**.

36 F. Kong, *et al.*, A Conjugated Microporous Polymer/Wood Aerogel with Physical Adsorption, Chemical Degradation and Antibacterial Self-Cleaning Triple Sewage Treatment Functions, *Polymers*, 2023, **15**(19), 3929, DOI: **10.3390/polym15193929**.

37 Q. W. Cao, Y. F. Zheng and X. C. Song, Enhanced visible-light-driven photocatalytic degradation of RhB by $AgIO_3$/WO_3 composites, *J. Taiwan Inst. Chem. Eng.*, 2017, **70**, 359–365, DOI: **10.1016/j.jtice.2016.10.030**.

38 C. Yao, *et al.*, Probing the facet-dependent intermediate in the visible-light degradation of RhB by carbon-coated anatase TiO_2 nanoparticles, *J. Alloys Compd.*, 2020, **846**, 156335, DOI: **10.1016/j.jallcom.2020.156335**.

39 Y. Song, J. Lu, M. Li, Y. Yan and N. Zuo, Enhancing photocatalytic degradation of La-$BiVO_4$ through bidirectional regulation of oxygen vacancy and the Mott-Schottky effect, *Surf. Interfaces*, 2024, **54**, 105121, DOI: **10.1016/j.surfin.2024.105121**.

40 L. A. Luu Thi, *et al.*, In Situ g-C_3N_4@ZnO Nanocomposite: One-Pot Hydrothermal Synthesis and Photocatalytic Performance under Visible Light Irradiation, *Adv. Mater. Sci. Eng.*, 2021, **2021**, 17–20, DOI: **10.1155/2021/6651633**.

41 Z. Khalid, *et al.*, Causonis trifolia-based green synthesis of multifunctional silver nanoparticles for dual sensing of mercury and ferric ions, photocatalysis, and biomedical applications, *RSC Adv.*, 2025, **15**(21), 16879–16893, DOI: **10.1039/d5ra01882j**.

42 A. B. Siddique, M. A. Shaheen, A. Abbas, Y. Zaman, H. M. A. Amin, M. M. Alam, N. K. Alharbi, F. Alshehri, A. Shami, F. A. Al-Joufi and A. Ali, Sunlight-assisted greenly synthesised silver nanoparticles for highly selective mercury ion sensing, biomedical and photocatalytic applications, *Int. J. Environ. Anal. Chem.*, 2025, 1–23, DOI: **10.1080/03067319.2025.2502605**.

43 Y. Chen, *et al.*, Construction of Ag decorated P-doped g-C_3N_4 nanosheets Schottky junction via silver mirror reaction for enhanced photocatalytic activities, *Int. J. Hydrogen Energy*, 2022, **47**(1), 250–263, DOI: **10.1016/j.ijhydene.2021.10.024**.

44 S. Zhang, *et al.*, Hybrid 0D-2D Nanoheterostructures: In Situ Growth of Amorphous Silver Silicates Dots on g-C_3N_4 Nanosheets for Full-Spectrum Photocatalysis, *ACS Appl.*

Mater. Interfaces, 2016, **8**(51), 35138–35149, DOI: **10.1021/acsami.6b09260**.

45 M. E. Khan, T. H. Han, M. M. Khan, M. R. Karim and M. H. Cho, Environmentally sustainable fabrication of Ag@g-C₃N₄ nanostructures and their multifunctional efficacy as antibacterial agents and Photocatalysts, *ACS Appl. Nano Mater.*, 2018, **1**(6), 2912–2922, DOI: **10.1021/acsanm.8b00548**.

46 K. Mallikarjuna, *et al.*, Sono-chemical synthesis of silver quantum dots immobilized on exfoliated graphitic carbon nitride nanostructures using ginseng extract for photocatalytic hydrogen evolution, dye degradation, and antimicrobial studies, *Nanomaterials*, 2021, **11**(11), 2918, DOI: **10.3390/nano11112918**.

47 Y. Orooji, M. Ghanbari, O. Amiri and M. Salavati-Niasari, Facile fabrication of silver iodide/graphitic carbon nitride nanocomposites by notable photo-catalytic performance through sunlight and antimicrobial activity, *J. Hazard. Mater.*, 2020, **389**, 122079, DOI: **10.1016/j.jhazmat.2020.122079**.